5. Bartlett, P. A. & Satake, K. Does dehydroquinate synthase synthesize dehydroquinate? *J. Am. Chem. Soc.* **110,** 1628–1630 (1988).
6. Lambert, J. M., Boocock, M. R. & Coggins, J. R. The 3-dehydroquinate synthase activity of the pentafunctional arom enzyme complex of *Neurospora crassa* is Zn^{2+} dependent. *Biochem. J.* **226,** 817–829 (1985).
7. Montchamp, J.-L. & Frost, J. W. Cyclohexenyl and cyclohexylidene inhibitors of 3-dehydroquinate synthase: Active site interactions relevant to enzyme mechanisms and inhibitor design. *J. Am. Chem. Soc.* **119,** 7645–7653 (1997).
8. Bentley, R. The shikimate pathway—a metabolic tree with many branches. *Crit. Rev. Biochem. Mol. Biol.* **25,** 307–384 (1990).
9. Kishore, G. M. & Shah, D. M. Amino acid biosynthesis inhibitors as herbicides. *Annu. Rev. Biochem.* **57,** 27–63 (1988).
10. Pittard, A. J. Biosynthesis of aromatic amino acids. *Escherichia coli and Salmonella typhimurium: Cellular and Molecular Biology* (eds Niedhardt, F. C. *et al.*) **1,** 368–394 (Am. Soc. Microbiol., Washington, DC, 1987).
11. Günel-Özcan, A., Brown, K. A., Allen, A. & Maskell, D. J. *Salmonella typhimurium aroB* mutants are attenuated in BALB/c mice. *Microbial Pathogen.* **17,** 169–174 (1997).
12. Case, M. E. & Giles, N. H. Partial enzyme aggregates formed by pleiotropic mutants in the arom gene cluster of *Neurospora crassa*. *Proc. Natl. Acad. Sci. USA* **68,** 58–62 (1971).
13. Hawkins, A. R., Lamb, H. K., Moore, J. D., Charles, I. G. & Roberts, C. F. The prechorismate (shikimate) and quinate pathways in filamentous fungi: theoretical and practical aspects. *J. Gen. Microbiol.* **139,** 2891–2899 (1993).
14. Rossmann, M. G., Moras, D. & Olsen, K. W. Chemical and biological evolution of a nucleotide-binding protein. *Nature* **250,** 194–199 (1974).
15. Lesk, A. M. NAD-binding domains of dehydrogenases. *Curr. Opin. Struct. Biol.* **5,** 775–783 (1995).
16. Kleywegt, G. J. & Jones, T. A. Where freedom is given, liberties are taken. *Structure* **3,** 535–540 (1995).
17. Holm, L. & Sander, C. Protein structure comparison by alignment of distance matrices. *J. Mol. Biol.* **233,** 123–138 (1993).
18. Murzin, A. G., Brenner, S. E., Hubbard, T. & Chothia, C. SCOP-A structural classification of proteins database for the investigation of sequences and structures. *J. Mol. Biol.* **247,** 536–540 (1995).
19. Eklund, H. *et al*. Three-dimensional structure of horse liver alcohol dehydrogenase at 2.4 Å resolution. *J. Mol. Biol.* **102,** 27–59 (1976).
20. Eklund, H. *et al*. Structure of the triclinic ternary complex of horse liver alcohol dehydrogenase at 2.9 Å resolution. *J. Mol. Biol.* **146,** 561–587 (1981).
21. Van Den Hombergh, J. P. T. W., Moore, J. D., Charles, I. G. & Hawkins, A. R. Overproduction in *Escherichia coli* of the dehydroquinate synthase domain of the *Aspergillus nidulans* pentafunctional AROM protein. *Biochem. J.* **284,** 861–867 (1992).
22. Moore, J. D., Coggins, J. R., Virden, R. & Hawkins, A. R. Efficient independent activity of a monomeric, monofunctional dehydroquinate synthase derived from the N-terminus of the penta-functional AROM protein of *Aspergillus nidulans*. *Biochem. J.* **301,** 297–304 (1994).
23. Otwinowski, Z. & Minor, W. Processing of X-ray diffraction data collected in oscillation mode. *Meth. Enzymol.* **276,** 307–326 (1996).
24. The CCP4 suite: programs for protein crystallography. *Acta Crystallogr. D* **50,** 760–763 (1994).
25. Terwilliger, T. C., Kim, S.-H. & Eisenberg, D. Generalised method of determining heavy atom positions using the difference Patterson function. *Acta Crystallogr. A* **43,** 1–5 (1987).
26. Jones, T. A., Zou, J.-Y., Cowan, S.W. & Kjeldgaard, M. Improved methods for building protein models in electron-density and the location of errors in these models. *Acta Crystallogr. A* **47,** 110–119 (1991).
27. Tronrud, D. E., *The TNT Refinement Package Manual*, 1–191, Oregon State Board of Higher Education (1993).
28. Brunger, A. T. Free *R*-value—a novel statistical quantity for assessing the accuracy of crystal structures. *Nature* **355,** 472–475 (1992).
29. Esnouf, R. M. An extensively modified version of Molscript that includes greatly enhanced coloring capabilities. *J. Mol. Graph. Model.* **15,** 132 (1997).

Acknowledgements. We thank the support staff at the Synchrotron Radiation Source at Daresbury Laboratory, UK, for assistance; D. R. Swatman, F.T.F. Tsai, R. R. Patel and Y. S. Li for technical assistance; G. G. Dodson for support and encouragement; K. Henrick, S. Gamblin, M. Hirschberg, J. O. Baum, W. Taylor and J. D. Moore for discussion; and P. Bartlett for helpful comments. This work was supported by BBSRC. E.P.C. was supported by the UK MRC and K.A.B. received a BBSRC Advanced Fellowship.

Correspondence and requests for materials should be addressed to K.A.B. (e-mail: k.brown@ic.ac.uk).
Coordinates have been deposited with the Brookhaven Databank under accession number 1dqs.

addendum

A prolactin-releasing peptide in the brain

Shuji Hinuma, Yugo Habata, Ryo Fujii, Yuji Kawamata, Masaki Hosoya, Shoji Fukusumi, Chieko Kitada, Yoshinori Masuo, Tsuneo Asano, Hirokazu Matsumoto, Masahiro Sekiguchi, Tsutomu Kurokawa, Osamu Nishimura, Haruo Onda & Masahiko Fujino

Nature **393,** 272–276 (1998)

The prolactin-releasing peptide cDNA sequence data have been submitted to the DDBJ/EMBL/GenBank databases. The accession numbers are as follows: AB015417, *Bos taurus* mRNA for pre-proprolactin-releasing peptide; AB015418, *Rattus norvegicus* mRNA for preproprolactin-releasing peptide; AB015419, *Homo sapiens* mRNA for preproprolactin-releasing peptide. □

correction

Engineering cyclophilin into a proline-specific endopeptidase

Eric Quéméneur, Mireille Moutiez, Jean-Baptiste Charbonnier & André Ménez

Nature **391,** 301–304 (1998)

The efficiency value (k_{cat}/K_m) of cyprase 1 is equal to $0.2 \times 10^4\,M^{-1}\,s^{-1}$, and not to $0.7 \times 10^4\,M^{-1}\,s^{-1}$ as published. Also, the histidine at residue 104 titrates with a pK equal to 6.47 ± 0.16 and 6.74 ± 0.15 when measuring K_{cat} and the k_{cat}/K_m, respectively, and not to 6.74 ± 0.16 and 6.74 ± 0.15. □

$V_5)/V_6\}$, and, in mV, $V_1 = -42.5$, $V_2 = -1$, $V_3 = -43.0$, $V_4 = -4$, $V_5 = -60.0$, and $V_6 = 64$. Simulation results were obtained by numerical integration of differential equations over 10 s.

Bipolar-neuron model. See Fig. 2a. The soma was the same as in the point-neuron model (20 μm diameter, $R_{soma} = 135\,M\Omega$); the dendritic diameter was either 4 μm (thick dendrites) or 2 μm (thin dendrites), with axial resistivity $R_i = 200\,\Omega$ cm and membrane resistance $R_m = 1{,}700\,\Omega\,cm^2$. For a dendrite of diameter 4 μm, $\lambda = 290$ μm, whereas for a dendrite of diameter 2 μm, $\lambda = 200$ μm. Parameters were based on recordings from chicken coincidence detectors[20]. Dendrites were modelled by 0.05-λ-connected compartments and had either active membrane (identical to the point neuron) or passive membrane (voltage-dependent conductances fixed to their resting values). Because synaptic inputs arrived at the cell in every cycle, it was insufficient to use a simple threshold function to recognize action potentials in the somatic response. We therefore added a long axon with a higher density of voltage-dependent conductances. We counted only action potentials that propagated.

Synaptic-input model. See Fig. 2b. For every input train, at every stimulus cycle, the probability of an input arriving was defined as f_{pre}/f_{stim}, where f_{stim} was the stimulus frequency and f_{pre} ($\leqslant f_{stim}$) was the average spike rate of the input train. $f_{pre} = 350$ Hz for all stimulus frequencies[27]. The stimulus cycles were regulated as independent events. To account for the jitter in the phase-locking of the inputs to the stimulus, measured by vector strength (VS)[3], we shifted each input in time from the beginning of the cycle by a random variable $t_{shift} \sim N(m = 0, \sigma = (1{,}000/f_{stim})\{\sqrt{-2\ln(VS)}/(2\pi)\}$ ms). For $VS \geqslant 0.2$, this resulted in input trains with the required VS. Except in Fig. 1d, we used $VS = 0.7$. In Fig. 1d, $VS = 0.8$. Synaptic inputs were rectangular conductance changes, 0.4 ms wide.

Bipolar integrate-and-fire model. The probability that the coincidence-detector neuron would fire in a given stimulus cycle was assumed to be $P(g_L, g_R) = 1/(1 + \exp[\{1 - (g_L/g_{Th})^\alpha - (g_R/g_{Th})^\alpha\}/k])$, where g_L and g_R were the total synaptic input conductance during this cycle from the left and right ears, respectively. We used $k = 0.05$ and $g_{Th} = 1$ (the positive parameter k determines the steepness of the sigmoid threshold function). By using a sigmoid $P(g_L, g_R)$ (rather than the condition $g_L^\alpha + g_R^\alpha \geqslant g_{Th}^\alpha$, which is equivalent to the sigmoidal function when k approaches 0), we approximately accounted for the effects of small intrinsic noise, jitter in a composite input, and a graded threshold for the spike-generating mechanism. The probability $b_{i,n}$ (see text) was calculated by $b_{i,n} = \binom{n}{i}(f_{pre}/f_{stim})^i(1 - f_{pre}/f_{stim})^{n-i}$. Then, P_0 is

$$P_0 = \sum_{i=0}^{n}\sum_{j=0}^{n} b_{i,n}b_{j,n}P(ig_{syn}, jg_{syn})$$

where input combinations are summed with index i for the left side and j for the right. On the other hand, if the binaural phase shift was 180°, the probability to fire during one cycle (that is, the probability that inputs from the left or the right ear will cause firing) was approximated by

$$P_{180} = 2\sum_{i=0}^{n} b_{i,n}P(ig_{syn}, 0)$$

provided that P_{180} was small enough. In the modified version of the model, the jitter was accounted for by using instead

$$P_{180} = 2\sum_{i=0}^{n}\sum_{j=0}^{n} b_{i,n}b_{j,n}P(ig_{syn}, \beta jg_{syn})$$

Received 7 January; accepted 16 March 1998.

1. Jeffress, L. A. A place theory of sound localization. *J. Comp. Physiol. Psychol.* **41,** 35–39 (1948).
2. Carr, C. E. Timing mechanisms in the CNS. *Annu. Rev. Neurosci.* **16,** 223–243 (1993).
3. Goldberg, J. M. & Brown, P. B. Response of binaural neurons of dog superior olivary complex to dichotic tonal stimuli: some physiological mechanisms of sound localization. *J. Neurophysiol.* **32,** 613–636 (1969).
4. Carr, C. E. & Konishi, M. A circuit for detection of interaural time differences in the brainstem of the barn owl. *J. Neurosci.* **10,** 3227–246 (1990).
5. Overholt, E. M., Rubel, E. W. & Hyson, R. L. A delay-line circuit for coding interaural time differences in the chick brain stem. *J. Neurosci.* **12,** 1698–1708 (1992).
6. Yin, T. C. T. & Chan, J. C. K. Interaural time sensitivity in the medial superior olive of the cat. *J. Neurophysiol.* **64,** 465–488 (1990).
7. Smith, Z. D. J. & Rubel, E. W. Organization and development of brain stem auditory nuclei of the chicken: dendritic gradients in nucleus laminaris. *J. Comp. Neurol.* **186,** 213–239 (1979).
8. Stotler, W. A. An experimental study of the cells and connections of the superior olivary complex of the cat. *J. Comp. Neurol.* **98,** 401–432 (1953).
9. Segev, I., Rinzel, J. & Sheperd, G. *The Theoretical Foundation of Dendritic Function: Selected Papers of Wilfrid Rall with Commentaries* (MIT Press, Cambridge, MA, 1995).
10. Mel, B. Information processing in dendritic trees. *Neural Comp.* **6,** 1031–1085 (1994).
11. Segev, I. in *The Handbook of Brain Theory and Neural Networks* (ed. Arbib, M.) 282–289 (MIT Press, Cambridge, MA, 1995).
12. Pinsky, P. F. & Rinzel, J. Intrinsic and network rhythmogenesis in a reduced Traub model for CA3 neurons. *J. Comput. Neurosci.* **1,** 39–40 (1994).
13. Mainen, Z. F. & Sejnowski, T. J. Influence of dendritic structure on firing pattern in model neocortical neurons. *Nature* **382,** 363–366 (1996).
14. Softky, W. R. & Koch, C. The highly irregular firing of cortical cells in inconsistent with temporal integration of random EPSPs. *J. Neurosci.* **13,** 334–350 (1993).
15. Borst, A. & Egelhaaf, M. Dendritic processing of synaptic information by sensory interneurons. *Trends Neurosci.* **17,** 257–263 (1994).
16. Borst, A. How do nerve cells compute? Dendritic integration in fly visual neurons. *Acta Physiol. Scand.* **157,** 403–407 (1996).
17. Haag, J. & Borst, A. Amplification of high-frequency synaptic inputs by active dendritic membrane processes. *Nature* **379,** 639–641 (1996).
18. Parks, T. N. & Rubel, E. W. Organization of the projections from n. magnocellularis to n. laminaris. *J. Comp. Neurol.* **180,** 439–448 (1975).
19. Reyes, A. D., Rubel, E. W. & Spain, W. J. Membrane properties underlying the firing of neurons in the avian cochlear nucleus. *J. Neurosci.* **14,** 5352–5364 (1994).
20. Reyes, A. D., Rubel, E. W. & Spain, W. J. *In vitro* analysis of optimal stimuli for phase-locking and time-delayed modulation of firing in avian nucleus laminaris neurons. *J. Neurosci.* **16,** 993–1000 (1996).
21. Zhang, S. & Trussell, L. O. A characterization of excitatory postsynaptic potentials in the avian nucleus magnocellularis. *J. Neurophysiol.* **72,** 705–718 (1994).
22. Manis, P. B. & Marx, S. O. Outward currents in isolated ventral cochlear nucleus neurons. *J. Neurosci.* **11,** 2865–2880 (1991).
23. Agmon-Snir, H., Carr, C. E. & Rinzel, J. A simple biophysical model for analyzing phase-locking and coincidence detection inauditory neurons. *Soc. Neurosci. Abstr.* **22,** 402 (1996).
24. Colburn, H. S., Han, Y. & Culotta, C. P. Coincidence model of MSO responses. *Hearing Res.* **49,** 335–346 (1990).
25. Brughera, A. R., Stutman, E. R., Carney, L. H. & Colburn, H. S. A model with excitation and inhibition for cells in the medial superior olive. *Aud. Neurosci.* **2,** 219–233 (1996).
26. Gerstner, W., Kempter, R., Van Hemmen, J. L. & Wagner, H. A neuronal learning rule for submillisecond temporal coding. *Nature* **383,** 76–78 (1996).
27. Warchol, M. E. & Dallos, P. Neural coding in the chick cochlear nucleus. *J. Comp. Physiol.* **166,** 721–734 (1990).
28. Morris, C. & Lecar, H. Voltage oscillations in the barnacle giant muscle fiber. *Biophys. J.* **35,** 193–213 (1981).
29. Rinzel, J. & Ermentrout, G. B. in *Methods in Neuronal Modeling: from Synapses to Networks* (eds Koch, C. & Segev, I.) 135–169 (MIT Press, Cambridge, MA, 1989).
30. Smith, P. H. Structural and functional differences distinguish principal from nonprincipal cells in the guinea pig MSO slice. *J. Neurophysiol.* **73,** 1653–1667 (1995).

Acknowledgements. This work was supported by grants from the NIH (to C.E.C.) and the Human Frontier Science Program (to H.A.-S.). We thank G. Gerstein, I. Nelken, E. W. Rubel, D. Sanes and I. Segev for comments, and the NCI Biomedial Supercomputing Center at Frederick for computer resources and technical help.

Correspondence and requests for materials should be addressed to C.E.C. (e-mail: carr@zool.umd.edu).

A prolactin-releasing peptide in the brain

Shuji Hinuma*, Yugo Habata*, Ryo Fujii*, Yuji Kawamata*, Masaki Hosoya*, Shoji Fukusumi*, Chieko Kitada*, Yoshinori Masuo*, Tsuneo Asano†, Hirokazu Matsumoto*, Masahiro Sekiguchi‡, Tsutomu Kurokawa*, Osamu Nishimura†, Haruo Onda* & Masahiko Fujino*

** Discovery Research Laboratories I, Pharmaceutical Discovery Research Division, † Pharmaceutical Research Division, and ‡ Pharmaceutical Development Division, Takeda Chemical Industries Ltd, 10 Wadai, Tsukuba, Ibaraki 300-4293, Japan*

Hypothalamic peptide hormones regulate the secretion of most of the anterior pituitary hormones, that is, growth hormone, follicle-stimulating hormone, luteinizing hormone, thyroid-stimulating hormone and adrenocorticotropin[1,2]. These peptides do not regulate the secretion of prolactin[1,2], at least in a specific manner, however. The peptides act through specific receptors, which are referred to as seven-transmembrane-domain receptors or G-protein-coupled receptors[3–7]. Although prolactin is important in pregnancy and lactation in mammals, and is involved in the development of the mammary glands and the promotion of milk synthesis[8,9], a specific prolactin-releasing hormone has remained unknown. Here we identify a potent candidate for such a hormone. We first proposed that there may still be unknown peptide hormone factors that control pituitary function through seven-transmembrane-domain receptors. We isolated the

complementary DNA encoding an 'orphan' receptor (that is, one for which the ligand is unknown). This receptor, hGR3, is specifically expressed in the human pituitary. We then searched for the hGR3 ligand in the hypothalamus and identified a new peptide, which shares no sequence similarity with known peptides and proteins, as an endogenous ligand. We show that this ligand is a potent prolactin-releasing factor for rat anterior pituitary cells; we have therefore named this peptide prolactin-releasing peptide.

We searched seven-transmembrane-domain receptors (7TMRs) with a polymerase chain reaction (PCR) method, and isolated from the human pituitary an orphan 7TMR, hGR3, that is nearly identical to GPR10 (ref. 10) and a human counterpart of rat UHR-1 (ref. 11). Quantitative analyses of UHR-1 messenger RNA by reverse transcription PCR (RT-PCR) revealed that, of over 40 different tissues, the pituitary expressed UHR-1 mRNA at the highest level, whereas the brain, spinal cord, adrenal gland, and femur expressed UHR-1 mRNA at moderate levels. *In situ* hybridization analysis indicated that the anterior lobe abundantly expressed UHR-1 mRNA, suggesting that UHR-1 or hGR3 is particularly important in the regulation of anterior pituitary function.

On the basis of specific signal transduction in CHO cells expressing hGR3 (CHO-19P2) compared with in CHO cells transfected with a vector plasmid lacking hGR3 cDNA, we searched for an endogenous ligand of hGR3 in tissue extracts. We used several different assays for detecting signal transduction, and detected a specific response of CHO-19P2 cells to bovine hypothalamic extract when we used the arachidonic acid metabolite release assay. We used this assay as the basis for the purification of an hGR3 ligand through a combination of chromatographic procedures. The arachidonic acid metabolite-releasing activities separated into three peaks (P1, P2 and P3) with Vydac C_{18} column chromatography. As the activity of P1 seemed to be less than those of P3 and P2, we purified P3 and P2 by Vydac diphenyl column and μRPC C_2/C_{18} column chromatography. As shown in Fig. 1a, two peaks of activity further separated from P3 by μRPC C_2/C_{18} column chromatography. Both peaks derived from P3 gave the same partial amino-terminal

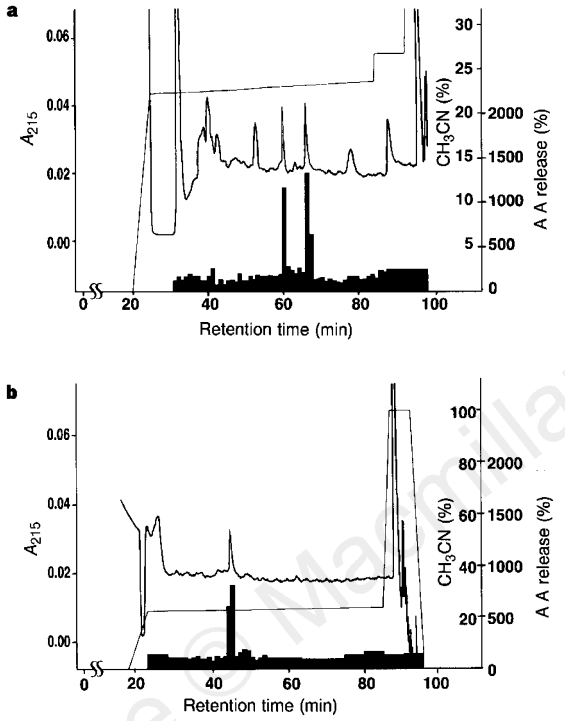

Figure 1 Purification of peptide ligands for hGR3 from bovine hypothalamic extract. The arachidonic acid metabolite (AA)-releasing activity (black areas) of each fraction is expressed as a percentage of the amount of [^{3}H]AA released from control CHO-19P2 cells in a single assay. Thick jagged trace, A_{215}; thin line, percentage of CH_3CN. **a**, The profile of peptide P2 in μRPC C_2/C_{18} column chromatography using a SMART system. Elution was performed with a linear gradient of 22.0–23.5% CH_3CN. **b,** The profile of peptide P2 in μRPC C_2/C_{18} column chromatography with a linear gradient of 21.5–23.0% Ch_3CN.

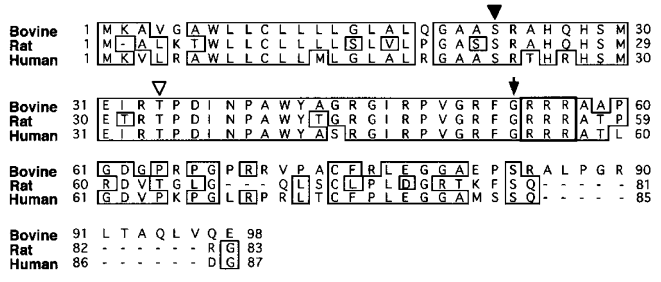

Figure 2 Amino-acid sequences of bovine, rat and human preproproteins containing PrRP. These sequences were deduced from cDNAs. The filled and open arrowheads indicate the N termini of PrRP31 and PrRP20, respectively. The arrow indicates a glycine residue that is presumed to react as an amide donor. The triplets of basic amino-acid residues that constitute the typical motif of a proteolytic cleavage site are boxed with a thick line. Amino-acid residues with identical sequence in at least two of the species are boxed with a thin line.

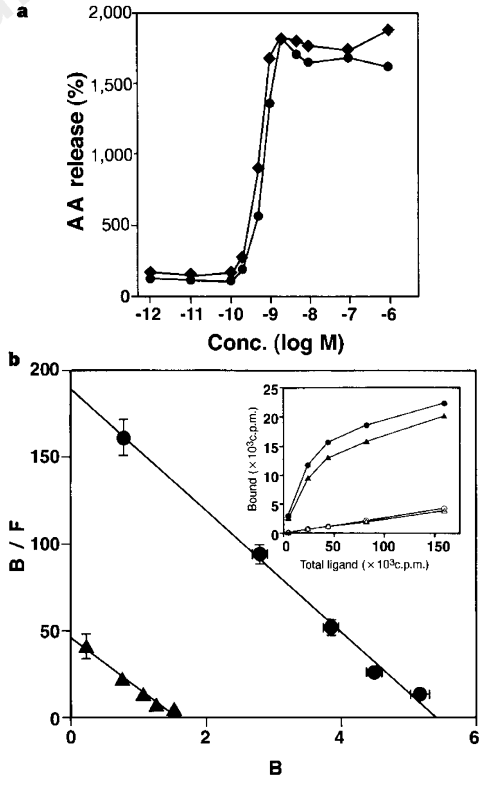

Figure 3 Specific interaction of synthetic PrRPs with hGR3 and UHR-1. **a**, Specific arachidonic acid metabolite (AA) release from CHO-19P2 cells is induced by PrRPs. CHO-19P2 cells were incubated with the indicated concentrations of bovine PrRP31 (circles) or PrRP20 (diamonds), respectively. Values represent the means of percentages of [^{3}H]AA released in relation to a control in duplicate assays. The amount of [^{3}H]AA released from the control was 867 c.p.m. **b**, Scatchard analysis of the binding of bovine PrRP31 to hGR3 and UHR-1. Scatchard plots of binding of ^{125}I-labelled bovine PrRP31 to CHO-19P2 (circles) and CHO-UHR-1 (triangles) cells are shown. B, bound (p mol mg^{-1} protein); F, free (nM). The inset panel represents the saturation binding data: symbols indicate the total binding of ^{125}I-labelled bovine PrRP31; in the presence of 1 μM unlabelled bovine PrRP31, to the membrane fraction of CHO-19P2 cells (filled circles) and CHO-UHR-1 cells (filled triangles), and nonspecific binding to CHO-19P2 cells (open circles) and CHO-UHR-1 cells (open triangles).

amino-acid sequence SRAHQHXMEIRTPDINPAXYAGRGIRPVG (X, unidentified residue), indicating that the difference between the two peaks might be due to a minor modification of the same peptide, such as oxidation of the methionine residue. In the case of P2, the activity was detected as a single peak (Fig. 1b). The purified P2 gave a partial N-terminal amino-acid sequence, which partly overlapped with that of P3, of TPDINPAWYAGRGIRPVGR.

We isolated bovine, rat and human cDNAs encoding the P2 and P3 peptide sequences from the brain of each species, using the purified peptide sequences as a basis for isolation of the cDNAs (Fig. 2). Although the bovine cDNA encoded a protein of 98 amino-acid residues, its N-terminal portion before Ser 23 showed the typical profile of a secretory signal peptide[12], indicating that P3 was generated through cleavage of the signal sequence. The P2 peptide sequence, which starts from Thr 34, indicates that the P2 peptide may be a truncated form of the P3 peptide. A typical proteolytic cleavage motif, comprising the basic amino-acid repeat Arg 55, Arg 56, Arg 57, was conserved among the species, as was Gly 54. This suggests that after cleavage between Gly 54 and Arg 55, Phe 53 at the carboxy terminus of the predicted mature peptides might be amidated by reacting with Gly 54 as an amide donor.

These results indicate that the preproprotein encoded by the bovine cDNA may generate at least two forms of mature peptide as naturally occurring endogenous ligands, that is, SRAHQHSM EIRTPDINPAWYAGRGIRPVGRF-NH_2 and TPDINPAWYAGRGIR PVGRF-NH_2, thought to correspond to the purified P3 and P2, respectively. We have named these peptides prolactin (PRL)-releasing peptides (PrRPs). PrRP31 and PrRP20 correspond to peaks P3 and P2, respectively. These putative mature peptide sequences were highly conserved among the species. We analysed the tissue distribution of PrRP mRNA in rats by the quantitative RT-PCR method, and found that the medulla oblongata expressed the highest level of PrRP mRNA, whereas the hypothalamus expressed PrRP mRNA at a moderate level. However, when determined on the basis of the arachindonic acid metabolite release assay, the content of bioactive PrRP in tissue extracts was highest in the hypothalamus.

We synthesized bovine, rat and human PrRP31 and PrRP20, and examined their ability to induce arachidonic acid metabolite release from CHO-19P2 cells and CHO cells expressing UHR-1 (CHO-UHR-1 cells). Synthetic PrRP31 and PrRP20 both promoted arachidonic acid metabolite release by CHO-19P2 (Fig. 3a) and CHO-UHR-1 cells, but not by mock-transfected CHO cells. We next examined the binding of synthetic PrRPs to hGR3 and UHR-1. ^{125}I-labelled bovine PrRP31 specifically bound to membrane fractions prepared from both CHO-19P2 and CHO-UHR-1 cells. Competitive binding experiments showed that unlabelled PrRPs inhibited the binding of ^{125}I-labelled bovine PrRP31 to both CHO-19P2 and CHO-UHR-1 cells, in a dose-dependent manner. As shown in Fig. 3b, Scatchard analysis showed that both CHO-19P2 and CHO-UHR-1 cells expressed a single class of high-affinity binding site for PrRP31. The dissociation constants (K_d) were 2.6×10^{-11} M and 2.5×10^{-11} M, and the maximal binding sites (B_{max}) were 4.8 and 1.3 pmol mg^{-1} protein, in CHO-19P2 and CHO-UHR-1 cells, respectively. However, PrRP31 with a non-

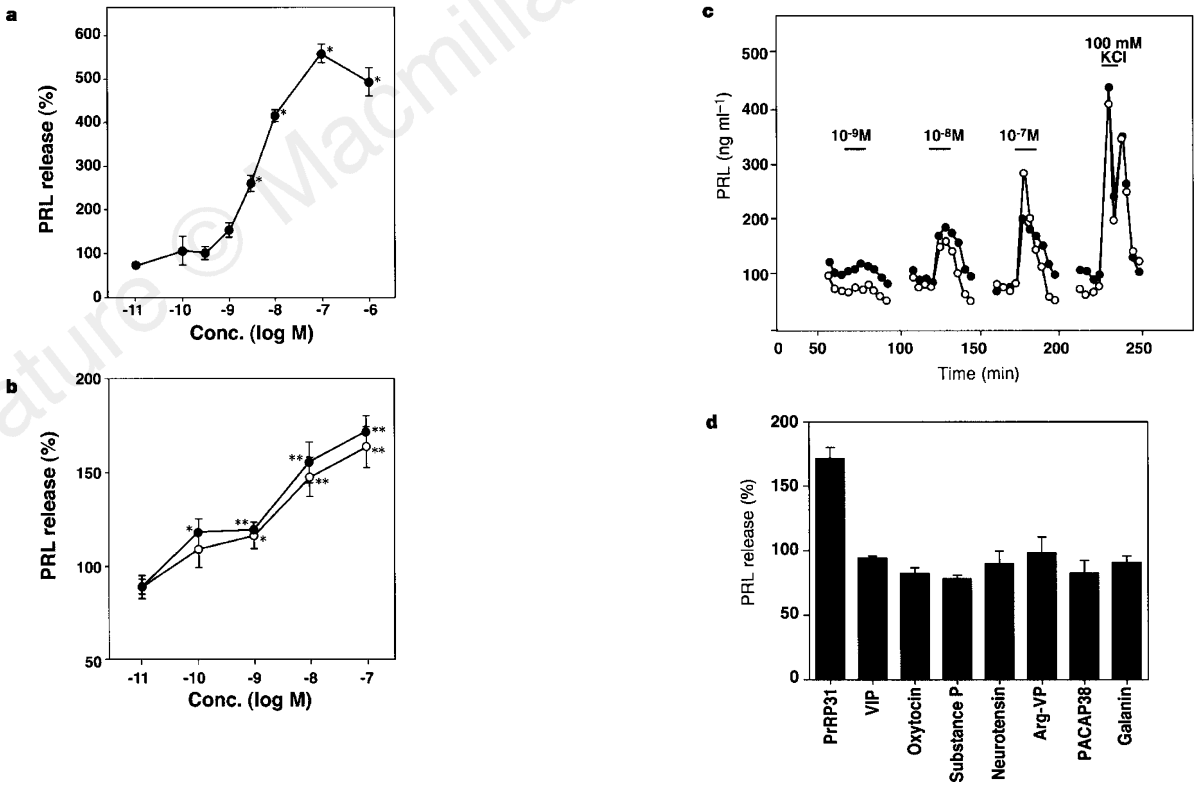

Figure 4 Promotion of PRL secretion from rat anterior pituitary cells by PrRP. **a**, Promotion of PRL secretion from RC-4B/C cells by bovine PrRP31. PRL concentrations represent the means of percentages ± s.e.m. (vertical bars) relative to a control (100%) without PrRP31, from quadruplicate assays. PRL released by the control was 1.2 ng ml^{-1}. **b**, Promotion of PRL secretion from primary cultured rat anterior pituitary cells in static incubation by bovine PrRP31. The indicated concentrations of bovine PrRP31 (filled circles) or TRH (open circles) were added to the culture. PRL concentrations are shown as for **a**. PRL released from the control was 518 ng ml^{-1}. **c**, Promotion of PRL secretion from rat anterior pituitary cells by rat PrRP31 in a perifusion assay. Rat PrRP31 (filled circles) and TRH (open circles) at indicated doses were added to the system in different chambers at the intervals indicated by the horizontal bars. PRL concentrations taken every 3 min are indicated. **d**, Comparison of the ability of PrRP and of known peptides to promote PRL secretion in static incubation. Bovine PrRP31 and the other peptides indicated were used at 10^{-7} M. VIP, vasoactive intestinal polypeptide; Arg-VP, arginine–vasopressin; PACAP38, pituitary adenylate cyclase-activating polypeptide. Single asterisks indicate $P < 0.05$; double asterisks indicate $P < 0.01$ (when compared with control); Student's *t*-test.

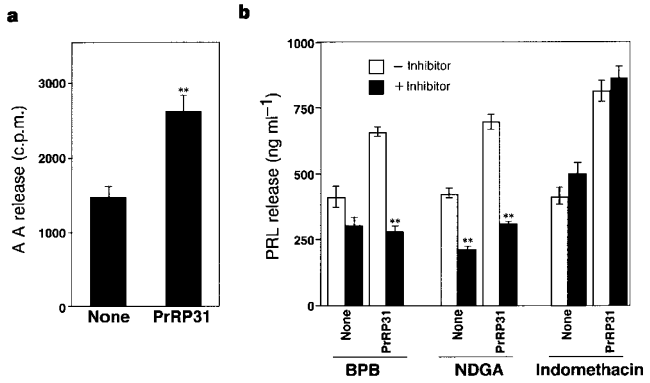

Figure 5 Relation between arachidonic acid metabolism and PRL secretion induced by PrRP in primary cultured rat anterior pituitary cells. Values represent the means of quadruplicate assays ± s.e.m. (vertical bars). Double asterisks indicate $P < 0.01$ (when compared with the control); Student's *t*-test. **a**, Release of arachidonic acid metabolites (AA) induced by rat PrRP31. AA release in the presence or absence (none) of rat PrRP31 at 10^{-7} M is shown. **b**, Effect of inhibitors on the secretion of PRL induced by rat PrRP31. Anterior pituitary cells untreated or treated with rat PrRP31 at 10^{-8} M were incubated in the presence (filled columns) or absence (white columns, controls) of each inhibitor at 50 μM.

amidated carboxyl group C terminus exhibited drastically decreased arachidonic acid metabolite-releasing and receptor-binding activities towards CHO-19P2 cells, indicating that an amidated C terminus is needed for PrRPs to interact with the receptor.

To determine the physiological effects of PrRP, we first studied its effect on a rat pituitary adenoma derived cell line, RC-4B/C[13], in which we had found the apparent expression of UHR-1 mRNA. Of the anterior pituitary hormones, only PRL was constitutively secreted at a detectable level by RC-4B/C cells under our culture conditions. Addition of PrRP31 to the culture increased the secretion of PRL from RC-4B/C cells within 30 min (Fig. 4a). We therefore expected that PrRP might act on lactotrophs to promote PRL secretion. We prepared anterior pituitary cells from lactating female rats, as the numbers of PRL-producing cells, that is, the lactotrophs, are increased in such rats[9]. We tested the effect of PrRP on hormone secretion from these cells. PrRP31 promoted PRL secretion within 15 min to 1 h of application (Fig. 4b). Thyrotropin-releasing hormone (TRH) is a potent factor that is known to be capable of promoting PRL secretion[8,9]; PrRP31 was comparable to TRH in its potency. However, PrRP31 did not influence the secretion of the other anterior pituitary hormones, that is, growth hormone, follicle-stimulating hormone, luteinizing hormone, thyroid-stimulating hormone or adrenocorticotropin. In addition, PrRP31 immediately promoted the secretion of PRL from rat anterior pituitary cells in a perifusion assay (Fig. 4c), indicating that PrRP may stimulate lactotrophs directly to secrete PRL. Although some other known peptides, such as vasoactive intestinal polypeptide, oxytocin, substance P, neurotensin, arginine–vasopressin, pituitary adenylate cyclase-activating polypeptide and galanin, have been reported to show PRL-releasing activity *in vitro* or *in vivo*[14–19], these peptides did not show apparent PRL-releasing activity in primary cultured rat anterior pituitary cells, at least under our experimental conditions (Fig. 4d).

Arachidonic acid metabolism is important as a signal-transduction pathway in PRL secretion by pituitary cells[20], although we found that PrRP could induce Ca^{2+} influx and a partial suppression of cyclic AMP production as well as arachidonic acid metabolite release in CHO-19P2 cells. As shown in Fig. 5a, PrRP induced pronounced arachidonic acid metabolite release as well as PRL secretion even in primary cultured rat anterior pituitary cells. In addition, as shown in Fig. 5b, the specific phospholipase A_2 inhibitor BPB (4-bromophenacylbromide) and the lipoxygenase inhibitor NDGA (nordihydroguaiaretic acid) attenuated both basal and PrRP-induced PRL secretion; however, the cycloxygenase inhibitor indomethacin had no such effect. These results show that arachidonic acid metabolism is closely linked to PrRP-induced PRL secretion, and that the lipoxygenase pathway is at least partly responsible for this effect.

The 7TMR gene family comprises many receptors which control various physiological functions. Many orphan 7TMRs have been discovered with the recent development of genome and cDNA research. However, only a few new peptide ligands have been identified for such orphan 7TMRs. Such peptides include orphanin FQ/nociceptin[21,22], a snail neuropeptide[23] and the orexins[24]. The strategy we used here would be applicable to the identification of many other unknown factors that regulate certain functions of various organs through orphan 7TMRs. The known hypothalamic hormones that regulate secretion of anterior pituitary hormones act on the pituitary through the hypophyseal portal vessel[1,2]. As levels of biologically active PrRP were highest in the hypothalamus, PrRP might also act on the anterior pituitary through the hypothalamus/portal vessel/pituitary axis, although this is uncertain at present. Further studies will be needed to reveal the physiological significance of PrRP and its receptor *in vivo*, but we observed that the levels of expression of the mRNA for PrRP and its receptor apparently fluctuate in the medulla oblongata and pituitary during pregnancy and lactation, respectively, in rats, indicating that levels of PrRP and its receptor are closely related to the regulation of certain reproductive processes. PRL secretion is regulated in a complicated manner *in vivo* in various physiological situations[8,9]. We assume that PrRP is important in the regulation of PRL secretion, especially in reproductive processes. PrRP and its receptor might also have functions in other tissues, including the central nervous system. Further studies of PrRP and its receptor will give us new insights into the regulatory mechanism of pituitary function and other physiological phenomena. □

Methods

Arachidonic acid metabolite release assay. We established CHO-19P2 and CHO-UHR-1 cells[5] by transfecting CHO cells lacking the dihydrofolate reductase gene with expression vector plasmids containing hGR3 or UHR-1 cDNAs. After culturing the CHO cells in 24-well plates at 5×10^4 cells per well for 24 h, and rat anterior pituitary cells in 24-well plates at 5×10^5 cells per well for 4 days, we added [^{3}H]arachidonic acid (NEN/Dupont) to each well at 0.25 or 2.0 μCi per well, and incubated the plates for a further 16 h. Then we washed the cells, added a sample, incubated the plates for 15 or 30 min, and measured the amount of [^{3}H]arachidonic acid released into the culture supernatant.

Purification of peptide ligands for hGR3. We boiled bovine hypothalamic tissue (2 kg), homogenized it in 1 M acetic acid, and collected the supernatant. We fractionated the supernatant on a C_{18} open column (PrepC_{18} 125Å:Waters) with stepwise increments of 10%, 30% and 50% CH_3CN in 0.05% trifluoroacetic acid (TFA) in water. We then fractionated the 30% CH_3CN fraction on HiPrep CM–Sepharose FF (Pharmacia), with stepwise increments of 100, 200, 500 and 1,000 mM CH_3COONH_4 (pH 6.4) in 10% CH_3CN. After precipitation with acetone, the 200 mM CH_3COONH_4 fraction was serially fractionated on a Resource RPC (Pharmacia) column with a linear gradient of 15–30% CH_3CN, a Resource S (Pharmacia) column with a linear gradient of 0–0.7 M NaCl in 50 mM 2-morpholinoethanesulphonic acid (pH 5) containing 10% CH_3CN, and a Vydac C_{18} 218TP5415 (Separations) column with a linear gradient of 20–30% CH_3CN. We further fractionated positive fractions (P3 and P2) on a Vydac diphenyl 219TP5415 (Separations) column with linear gradients of 22–25 and 21–24% CH_3CN for P3 and P2, respectively, and then

on a μRPC C_2/C_{18} SC 2.1/10 column (Pharmacia) in a SMART system (Pharmacia) for 60 min at a flow rate of 100 μl min^{-1}. We analysed the N-terminal amino-acid sequences of purified peptides with a protein sequencer (model 492, ABI).

Cloning of cDNAs encoding peptide ligands for hGR3. We isolated cDNA encoding the peptide ligands from poly(A)$^+$ RNA of the bovine hypothalamus by using PCR and rapid amplification of cDNA ends (RACE), with a 3′-RACE system (Gibco BRL), a Marathon cDNA amplification kit (Clontech), and degenerate primers designed on the basis of the purified peptide sequences. We isolated a rat cDNA from poly(A)$^+$ RNA prepared from the dorsal region of the medulla oblongata of Wistar rats, nearly according to the strategy used for the cloning of the bovine cDNA, and then isolated a human cDNA from human brain poly(A)$^+$ RNA (Clontech) with primers designed on the basis of conserved sequences found in bovine and rat cDNAs.

Synthesis of peptides. PrRPs were chemically synthesized with an automatic peptide synthesizer (model 430, ABI). They were also prepared as recombinant peptides produced in *Escherichia coli*[25,26]. Synthetic bovine PrRP31 was labelled with ^{125}I by use of [^{125}I] Bolton–Hunter reagent (NEN/Dupont). This PrRP was used for receptor-binding assays[27].

Assay for hormone secretions. RC-4B/C cells were cultured at 1×10^5 cells per well in 12-well tissue culture microplates for 2 days[13]. Anterior pituitary cells prepared from lactating female F344/N rats were cultured at 1.5×10^5 cells per well in poly-D-lysine-coated 24-well plates (Falcon Biocoat 40414) for 4 days[28]. The cells were then incubated with 1 ml of the medium containing each sample for 15 min to 1 h at 37 °C. Perifusion assays were performed at a flow rate of 0.33 ml min^{-1} (ref. 29). The PRL-secreting ability of the cells was confirmed by using KCl. Amounts of pituitary hormones were determined with assay kits (follicle-stimulating hormone, thyroid-stimulating hormone, luteinizing hormone, growth hormone and PRL, Biotrak RIA/Amersham; adrenocorticotropin, Nippon DPC).

Received 26 September 1997; accepted 26 March 1998.

1. Reichlin, S. Neuroendocrinology of the pituitary gland. *Toxicol. Pathol.* **17,** 250–255 (1989).
2. Koening, J. I. Pituitary gland: neurotransmitters and growth factors. *Toxicol. Pathol.* **17,** 256–265 (1989).
3. Mayo, K. E., Miller, T. L., Dealmeida, V., Zheng, J. & Godfrey, P. A. The growth hormone-releasing hormone receptor: signal transduction, gene expression, and physiological function in growth regulation. *Ann. NY Acad. Sci.* **805,** 184–203 (1996).
4. Kakar, S. S., Musgrove, L. C., Devor, D. C., Sellers, J. C. & Neill, J. D. Cloning, sequencing, and expression of human gonadotropin releasing hormone (GnRH) receptor. *Biochem. Biophys. Res. Commun.* **189,** 289–295 (1992).
5. Hinuma, S. *et al.* Molecular cloning and functional expression of a human thyrotropin-releasing hormone (TRH) receptor gene. *Biochim. Biophys. Acta* **1219,** 251–259 (1994).
6. Chalmers, D., Lovenberg, T. W., Grigoriadis, D. E., Behan, D. P. & De Souza, E. B. Corticotropin-releasing factor receptors: from molecular biology ot drug design. *Trends Pharmacol. Sci.* **17,** 166–172 (1996).
7. Patel, Y. C. *et al.* The somatostatin receptor family. *Life Sci.* **57,** 1249–1265 (1995).
8. Frantz, A. G. Prolactin. *N. Engl. J. Med.* **298,** 201–207 (1978).
9. Lamberts, S. W. & Macleod, R. M. Regulation of prolactin secretion at the level of the lactotroph. *Physiol. Rev.* **70,** 279–318 (1990).
10. Marchese, A. *et al.* Cloning and chromosomal maping of three novel genes, GPR9, GPR10, and GPR14, encoding receptors related to interleukin 8, neuropeptide Y, and somatostatin receptors. *Genomics* **29,** 335–344 (1995).
11. Welch, S. K., O'Hara, B. F., Kilduff, T. S. & Heller, H. C. Sequence and tissue distribution of a candidate G-coupled receptor cloned from rat hypothalamus. *Biochem. Biophys. Res. Commun.* **209,** 606–613 (1995).
12. Von Heijne, G. A new method for predicting signal sequence cleavage site. *Nucleic Acids Res.* **14,** 4683–4690 (1986).
13. Hurbain-Kosmath, I. *et al.* Gonadotropes in a novel rat pituitary tumor cell line, RC-4B/C. Establishment and partial characterization of the cell line. *In Vitro Cell. Dev. Biol.* **26,** 431–440 (1990).
14. Samson, W. K., Said, S. I., Snyder, G. & McCann, S. M. *In vitro* stimulation of prolactin release by vasoactive intestinal peptide. *Peptides* **1,** 325–332 (1980).
15. Samson, W. K., Lumpkin, M. D. & McCann, S. M. Evidence for a physiological role for oxytocin in the control of prolactin secretion. *Endocrinology* **119,** 554–560 (1986).
16. Rivier, C., Brown, M. & Vale, W. Effect of neurotensin, substance P and morphine sulfate on the secretion of prolactin and growth hormone in the rat. *Endocrinology* **100,** 751–754 (1977).
17. Erfurth, E. M., Hender, P., Lundin, S. & Ekman, R. Release of prolactin as well as adrenocorticotropin after administration of arginine-vasopression to healthy men. *Horm. Metab. Res.* **28,** 599–602 (1996).
18. Hammond, P. J. *et al.* Signalling pathways mediating secretory and mitogenic responses to galanin and pituitary adenylate cyclase-activating polypeptide in the 235-1 clonal rat lactotroph cell line. *J. Neuroendrocrinol.* **8,** 457–464 (1996).
19. Drouhault, R. *et al.* Prolactin and growth hormone release and calcium influx are stimulated by galanin within a 'window range' of concentrations in pituatary GH3 B6. *Neuroendrocrinol.* **60,** 179–184 (1994).
20. Canonico, P. L., Schettini, G., Vandenegro, C. A. & MacLeod, R. M. Arachidonic acid metabolism and prolactin secretion *in vitro*: a possible role for the lipoxygenase products. *Neuroendocrinol.* **37,** 212–217 (1983).
21. Reinscheid, R. K. *et al.* Orphanin FQ: a neuropeptide that activates an opioid-like G protein-coupled receptor. *Science* **270,** 792–794 (1995).
22. Meunier, J. C. *et al.* Isolation and structure of the endogenous agonist of opioid receptor-like ORL_1 receptor. *Nature* **377,** 532–535 (1995).
23. Cox, K. J. A. *et al.* Cloning, characterization, and expression of a G-protein-coupled receptor from *Lymnaea* stagnails and identification of a leucokninin-like peptide, PSFHSWSamide, as its endogenous ligand. *J. Neurosci.* **17,** 1197–1205 (1997).
24. Sakurai, T. *et al.* Orexins and orexin receptors: a family of hypothalamic neuropeptides and G protein-coupled receptors that regulate feeding behavior. *Cell* **92,** 575–585 (1998).
25. Koyama, N., Kuriyama, M., Amano, N. & Nishimura, O. A novel procedure for the preparation of biologically active recombinant peptides using a cyanylation reaction. *J. Biotechnol.* **32,** 273–281 (1994).
26. Nakagawa, S. *et al.* Chemical cleavage of recombinant fusion protein to yield peptide amides. *J. Am. Chem. Soc.* **116,** 5513–5514 (1994).
27. Miyamoto, Y. *et al.* Cloning and expression of a complementary DNA encoding the bovine receptor for pituitary adenylate cyclase-activating polypeptide (PACAP). *Biochim. Biophys. Acta* **1218,** 297–307 (1994).
28. Shiota, K. *et al. In vitro* thyrotroin release with thyrotropin-releasing hormone and an analogue, DN-1417. *Acta Endocrinol.* **106,** 71–78 (1984).
29. Hyde, J. F., Murai, I. & Ben-Jonathan, N. The rat posterior pituitary contains a potent prolactin-releasing factor: studies with perfused anterior pitutitary cells. *Endocrinology* **121,** 1531–1539 (1987).

Acknowledgements. We thank H. Okazaki and K. Tsukamoto for discussions throughout this study, and Y. Ishibashi, J. Noguchi, Y. Matsumoto, T. Moriya and M. Suenaga for collaboration.

Correspondence and requests for materials should be addressed to S.H. (e-mail: Hinuma_Shuji@takeda.co.jp).

Elastin is an essential determinant of arterial morphogenesis

Dean Y. Li*†, Benjamin Brooke†, Elaine C. Davis‡, Robert P. Mecham§, Lise K. Sorensen‖, Beth B. Boak‖, Ernst Eichwald¶ & Mark T. Keating*†‖

** Cardiology Division and ¶ Department of Pathology, University of Utah Health Sciences Center, Salt Lake City, Utah 84112, USA*
† Department of Human Genetics, Eccles Institute of Human Genetics and ‖ Howard Hughes Medical Institute, Salt Lake City, Utah 84112-5330, USA
‡ Department of Cell Biology and Neuroscience, University of Texas Southwestern Medical Center, Dallas, Texas 75235-9039, USA
§ Department of Cell Biology and Physiology and Department of Medicine, Washington University School of Medicine, St Louis, Missouri 63110, USA

Elastin, the main component of the extracellular matrix of arteries, was thought to have a purely structural role[1]. Disruption of elastin was believed to lead to dissection of arteries[2,3], but we showed that mutations in one allele encoding elastin cause a human disease in which arteries are blocked, namely, supravalvular aortic stenosis[4,5]. Here we define the role of elastin in arterial development and disease by generating mice that lack elastin. These mice die of an obstructive arterial disease, which results from subendothelial cell proliferation and reorganization of smooth muscle. These cellular changes are similar to those seen in atherosclerosis. However, lack of elastin is not associated with endothelial damage, thrombosis or inflammation, which occur in models of atherosclerosis. Haemodynamic stress is not associated with arterial obstruction in these mice either, as the disease still occurred in arteries that were isolated in organ culture and therefore not subject to haemodynamic stress. Disruption of elastin is enough to induce subendothelial proliferation of smooth muscle and may contribute to obstructive arterial disease. Thus, elastin has an unanticipated regulatory function during arterial development, controlling proliferation of smooth muscle and stabilizing arterial structure.

We isolated murine genomic clones encoding elastin (ELN) from a SV/129 λ FIX II library using an *ELN* complementary DNA clone. A targeting vector was constructed to delete 4.0 kilobases (kb) of the promoter and exon 1, resulting in a null mutation (Fig. 1a). The vector was electroporated into R1 embryonic stem cells and homologous recombinants were isolated by positive–negative selection[6]. Of 160 clones, we identified 3 as homologous recombinants by Southern blot analysis (Fig. 1b). These three clones were microinjected into C57BL/6 blastocysts and implanted in pseudopregnant

Phosphoamino-acid analysis, tryptic mapping, HPLC fractionation. 501mel cells were starved for 30 min in serum-free, phosphate-free RPMI medium, then labelled for 3 h using 1 mCi ml^{-1} ^{32}P-labelled inorganic phosphate. Cells were stimulated with Sl or TPA and solubilized in IP buffer. Mi proteins were immunoprecipitated overnight at 4 °C, electrophoresed and transferred to nitrocellulose. Bands were cut out and digested for 20 h at 37 °C with 25 μg TPCK-treated trypsin (Sigma). Phosphoamino-acid analysis and phosphopeptide mapping were carried out as described[14] using ammonium carbonate at pH 8.9. For HPLC fractionation, a 25-cm C18 reverse-phase column (Vydac) and an acetylnitrile gradient (0–70% in 0.1% trifluoroacetic acid) were used at a flow rate of 0.2 ml min^{-1}. Fractions were assayed by Cerenkov counting.

***In vitro* kinase assay.** Cells were activated and lysed and 4 μl of anti-Erk-2 antiserum (Santa Cruz) plus 20 μl protein-A–agarose beads were added to the lysate and mixed at 4 °C overnight. Beads were washed three times with lysis buffer and once with IVK buffer (50 mM HEPES, pH 7.6, 2 mM sodium vanadate, 10 mM magnesium chloride, 1 mM PMSF, 2 mM DTT and 50 μM ATP). For each reaction, 40 μl IVK buffer, 1 μl [γ-^{32}P]ATP, and phospho-acceptor protein were added. Myelin basic protein (5 μg) or Mi histidine fusion proteins spanning residues 16–185 or 139–419 (ref. 25) (4 μl of a solution having an absorbance of 0.065 at 280 nm) were added as substrates and incubated at 30 °C for 30 min. Reactions were stopped by addition of 2× SDS-sample buffer and analysed by western blot and autoradiography.

Luciferase assay. The human tyrosinase promoter reporter encompasses nucleotides −300 to +80 (ref. 16) in the pGL2Basic luciferase reporter (Promega). Wild-type Mi and the S73A mutant were cloned into the pEF-BOS expression vector[26]. The plasmid encoding constitutively active Raf was a 24G deletion mutant[27] (gift from G. Cooper). Wild-type MEK plasmid was a gift from L. Zon. Transfections were done by adding plasmid DNA (10 μg per 6-cm plate) to 300 μl DMEM, mixing 1:1 with a 5% lipofectamine/DMEM solution, and incubating at room temperature for 1 h. BHK cells maintained in DMEM/10% FCS were washed twice with serum-free DMEM before transfection. DNA/lipofectamine was added to 2 ml DMEM on a 6-cm plate. Cells were incubated overnight at 37 °C and fed the next morning, then collected for assay 8 h later and analysed with a Monolight 2010 luminometer using reagents as recommended by the manufacturer (Analytical Luminescence). Luciferase data were normalized to β-galactosidase activity in all samples.

Received 5 June; accepted 23 September 1997.

1. Moore, K. J. Insight into the microphthalmia gene. *Trends Genet.* **11,** 442–448 (1995).
2. Russell, E. Hereditary anemias of the mouse: a review for geneticists. *Adv. Genet.* **20,** 357–459 (1979).
3. Witte, O. Steel locus defines new multipotent growth factor. *Cell* **63,** 5–6 (1990).
4. Tassabehji, M., Newton, V. E. & Read, A. P. Waardenburg syndrome type 2 caused by mutations in the human microphthalmia (MITF) gene. *Nature Genet.* **8,** 251–255 (1994).
5. Hodgkinson, C. A. *et al.* Mutations at the mouse microphthalmia locus are associated with defects in a gene encoding a novel basic-helix-loop-helix-zipper protein. *Cell* **74,** 395–404 (1993).
6. Steingrimsson, E. *et al.* Molecular basis of mouse microphthalmia (mi) mutations helps explain their developmental and phenotypic consequences. *Nature Genet.* **8,** 256–263 (1994).
7. Hemesath, T. J. *et al. microphthalmia*, a critical factor in melanocyte development, defines a discrete transcription factor family. *Genes Dev.* **8,** 2770–2780 (1994).
8. Isozaki, K. *et al.* Cell type-specific deficiency of c-*kit* gene expression in mutant mice of mi/mi genotype. *Am. J. Path.* **145,** 827–836 (1994).
9. Dubreuil, P. *et al.* The c-*fms* gene complements the mitogenic defect in mast cells derived from mutant *W* mice but not *mi* (microphthalmia) mice. *Proc. Natl Acad. Sci. USA* **88,** 2341–2345 (1991).
10. Okuda, K. *et al.* Granulocyte-macrophage colony-stimulating factor, interleukin-3, and steel factor induce rapid tyrosine phosphorylation of p42 and p44 MAP kinase. *Blood* **79,** 2880–2887 (1992).
11. Marshall, C. Specificity of receptor tyrosine kinase signaling: transient versus sustained extracellular signal-regulated kinase activation. *Cell* **80,** 179–185 (1995).
12. Treisman, R. Regulation of transcription by MAP kinase cascades. *Curr. Opin. Cell Biol.* **8,** 205–215 (1996).
13. Ahn, N., Seger, R. & Krebs, E. The mitogen-activated protein kinase activator. *Curr. Opin. Cell Biol.* **4,** 992–999 (1992).
14. Boyle, W., van der Geer, P. & Hunter, T. Phosphopeptide mapping and phosphoamino acid analysis by two-dimensional separation on thin-layer cellulose plates. *Methods Enzymol.* **210,** 110–149 (1991).
15. Hearing, V. & Jiminiez, M. Mammalian tyrosinase—the critical regulatory control point in melanocyte pigmentation. *J. Biochem.* **19,** 1141–1147 (1987).
16. Bentley, N. J., Eisen, T. & Goding, C. R. Melanocyte-specific expression of the human tyrosinase promoter: activation by the microphthalmia gene product and role of the initiator. *Mol. Cell. Biol.* **14,** 7996–8006 (1994).
17. Yasumoto, K., Yokoyama, K., Shibata, K., Tomita, Y. & Shibahara, S. Microphthalmia-associated transcription factor as a regulator for melanocyte-specific transcription of the human tyrosinase gene [erratum, *Mol. Cell. Biol.* **15,** 1833 (1995)]. *Mol. Cell. Biol.* **14,** 8058–8070 (1994).
18. Costa, J. *et al.* Recombinant human stem cell factor (kit ligand) promotes human mast cell and melanocyte hyperplasia and functional activation *in vivo*. *J. Exp. Med.* **183,** 2681–2686 (1996).
19. Englaro, W. *et al.* Mitogen-activated protein kinase pathway and AP-1 are activated during cAMP-induced melanogenesis in B-16 melanoma cells. *J. Biol. Chem.* **270,** 24315–24320 (1995).
20. Bertolotto, C., Bille, K., Ortonne, J. & Ballotti, R. Regulation of tyrosinase gene expression by cAMP in B16 melanoma cells involves two CATGTG motifs surrounding the TATA box: implication of the microphthalmia gene product. *J. Cell Biol.* **134,** 747–755 (1996).
21. Ebi, Y. *et al.* Low c-kit expression of cultured mast cells of mi/mi genotype may be invovled in their defective responses to fibroblasts that express the ligand for c-kit. *Blood* **80,** 1454–1462 (1992).
22. Tsujimura, T. *et al.* Involvement of transcription factor encoded by the mi locus in the expression of c-kit receptor tyrosine kinase in cultured mast cells of mice. *Blood* **88,** 1225–1233 (1996).
23. Paulson, R., Vesey, S., Siminovitch, K. & Berstein, A. Signalling by the *W/Kit* receptor tyrosine kinase is negatively regulated by the protein tyrosine phosphatase Shp1. *Nature Genet.* **13,** 309–315 (1996).
24. Lorenz, U. *et al.* Genetic analysis reveals cell type-specific regulation of receptor tyrosine kinase c-Kit by the protein tyrosine phosphatase SHP1. *J. Exp. Med.* **184,** 1111–1126 (1997).
25. Tachibana, M. *et al.* Cloning of MITF, the human homolog of the mouse microphthalmia gene and assignment to chromosome 3p14.1–p12.3. *Hum. Mol. Genet.* **3,** 553–557 (1994).
26. Mizushima, S. & Nagata, S. pEF-BOS, a powerful mammalian expression vector. *Nucleic Acids Res.* **18,** 5322 (1990).
27. Stanton, V., Nichols, D., Laudano, A. & Cooper, G. Definition of the human *raf* amino-terminal regulatory region by deletion mutagenesis. *Mol. Cell. Biol.* **9,** 639–647 (1989).

Acknowledgements. We thank J. Jackson and J. Abraham for technical help, S. Galli, G. Cooper, M. Greenberg, B. Neel, D. Ron and P. Sharp for discussion, R. Halaban for 501mel cells, and members of the Burakoff laboratory for advice and assistance. This work was supported by grants from the NIH, the Pew Foundation, and the James S. McDonnell Foundation. T.J.H. is a Medical Foundation Fellow; D.E.F. is Nirenberg Fellow.

Correspondence and requests for materials should be addressed to D.E.F. (e-mail: david_fisher@dfci.harvard.edu).

Engineering cyclophilin into a proline-specific endopeptidase

Eric Quéméneur, Mireille Moutiez, Jean-Baptiste Charbonnier & André Ménez

Département d'Ingénierie et d'Etudes des Protéines, CEA Saclay, 91191 Gif-sur-Yvette, France

Designing an enzyme requires, among a number of parameters, the appropriate positioning of catalytic machinery within a substrate-binding cleft. Using the structures of cyclophilin–peptide complexes[1–4], we have engineered a new catalytic activity into an *Escherichia coli* cyclophilin by mutating three amino acids, close to the peptide binding cleft, to form a catalytic triad similar to that found in serine proteases. In conjunction with cyclophilin's specificity for proline-bearing peptides, this creates a unique endopeptidase, cyprose 1, which cleaves peptides on the amino-side of proline residues. When acting on an Ala-Pro dipeptide, cyprose 1 has an efficiency (k_{cat}/K_m) of 0.7×10^4 M^{-1} s^{-1} and enhances the rate of reaction (k_{cat}/k_{uncat}) 8×10^8-fold. This activity depends upon a deprotonated histidine and is inhibited by nucleophile-specific reagents, as occurs in natural serine proteases. Cyprose 1 can hydrolyse a protein substrate with a proline-specific endoprotease activity.

It is anticipated that protein engineering will allow the design of enzymes with new activities adapted to social and economical needs. However, only a few successes have paved this difficult avenue[5,6], probably because of the need for multiple complex determinants to be adjusted adequately for an efficient transition-state stabilization to occur[7]. These determinants include a substrate-binding cleft, the catalytic machinery and various parameters such as internal molecular dynamics and water molecules to mediate enzyme–ligand interactions. With the intention of engineering a proline-specific protease we tentatively grafted a proteolytic machinery into cyclophilin, which already possesses a binding cleft for peptidyl-prolyl substrates. Cyclophilins catalyse *cis–trans* isomerization of X-Pro bonds[8,9] but have never been reported to hydrolyse X-Pro bonds. As suggested by subtilisin mutants[10], the presence of a single nucleophilic serine at an appropriate distance from the carbonyl carbon of the substrate amide bond may produce some proteolysis, although presumably with a weak k_{cat} ($\leq 10^{-3}$ s^{-1}). Therefore, knowing the organization of X-Pro peptide-binding clefts of free[1] and peptide-bound cyclophilins[2–4], we mutated into serine a number of individual residues of the X-Pro binding pocket of ECypP, a cyclophilin from *E. coli*, and searched for a possible peptidase activity.

In the crystal structures[2–4], the β-carbons of R48, Q56, A91 and

T93 (as numbered in ECypP), are separated from the peptidyl X-Pro carbonyl carbon by distances ranging from 4.3 Å to 8.5 Å (Fig. 1). Although larger than the corresponding distance (3.2 Å) in serine protease–inhibitor complexes[11], we thought that these distances might accommodate any structural change that may result from mutations of selected residues into serine and may be compatible with any of the possible *cis* and/or *trans*-proline conformations of bound substrates. In this respect, several situations have been previously described which include the presence of a *cis* conformation in cyclophilin–peptide complexes[2–4] and a *trans* conformation in a Gly-Pro bond of a HIV1-gag hCyPA complex[12]. Also, although no *trans* X-Pro bonds (X being different from Gly) have ever been observed in crystal complexes, such conformers are most likely to be the main substrates of cyclophilins[4]. Therefore, the corresponding mutants were produced and their peptidase activity was measured using a chromophoric dipeptide furylacryloyl-alanylproline (fa-AP). The kinetic parameters were determined using both a spectrophotometric assay and a high-performance liquid chromatography (HPLC)-based method. The two techniques gave similar results. Table 1 shows that the wild-type ECypP, ECypP-R48S and ECypP-T93S had no detectable X-Pro peptidase activity ($k_{cat}/K_m < 10^{-3}\,s^{-1}\,M^{-1}$). In contrast, ECypP-Q56S and ECypP-A91S efficiently cleaved the substrate, the mutant A91S being more than 10^4-fold more potent than the mutant Q56S. Because we found that spontaneous hydrolysis of an fa-Ala-Pro bond occurs at a rate ($k_{uncat} = 4.8 \pm 0.9 \times 10^{-9}\,s^{-1}$) that is similar to that of other peptide bonds[13], our data demonstrate that the simple introduction of S91 in ECypP ($k_{cat} = 4.4 \pm 1.2 \times 10^{-2}\,s^{-1}$) enhanced by roughly 10^7-fold the rate constant of X-Pro bond cleavage. Therefore, both location and orientation of S91 and the pre-existing environment are favourable for ECypP to express a peptidase activity.

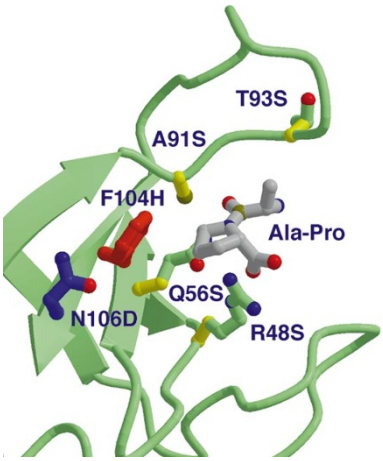

Figure 1 Enlarged view of the active site of an *E. coli* cyclophilin (PDB entry 1LOP[2]) illustrating the location of the Ala-Pro binding site and the enzyme residues selected for subsequent substitutions. In yellow are the Cα–Cβ bonds of four residues (R48, Q56, A91 and T93) which were converted into serine during the first round of mutagenesis. In red and blue are Phe 104 and Asn 106 subsequently converted into His and Asp, respectively. The drawings were made using MOLSCRIPT[23] and Raster3D[24].

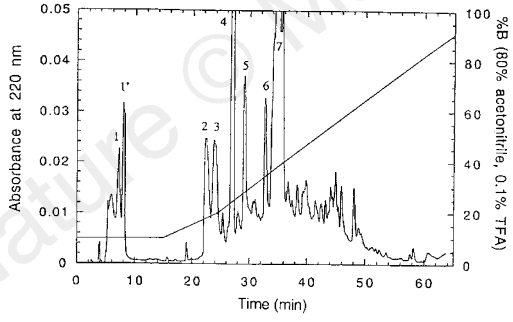

Peak number	N-terminal sequence	Measured mass	Theoretical mass	Fragment boundaries
2	LE*HNQQSSQ	1,169.75 ± 0.82	1,169.559	1-10
3	PGIKLN**TTD...	1,883.54 ± 0.96	1,884.066	47-61
4	PGETN*YKKV...	3,149.08 ± 0.53	3,149.740	18-42
5	PGETN*YKKVW...	5,544.23 ± 0.51	5,544.071	18-61
6	PGETNCYKKV...	3,549.62 ± 0.56	3,549.918	18-46
7	LECHNQQSSQPPT...	7,678.75 ± 0.88	7,677.162	1-61

Figure 2 Degradation of a protein by cyprose I. The major products resulting from enzymatic action of ECypP on a snake curaremimetic toxin (see Methods for experimental details) were separated by HPLC (top). Eight fractions whose absorbance (A_{220}) is higher than 0.15 were numbered from 1 to 7. They were analysed by Edman sequencing and electron spray mass spectrometry with the results given in the table (bottom). Fractions 1 and 1′ were non-peptidic compounds. The reaction yield was 25% as determined from the proportion of remaining non-hydrolysed toxin (peak 7). Cleavages occurred before Pro 11 (peak 2), Pro 18 (peaks 4, 5 and 6), Pro 43 (peak 4) and Pro 47 (peaks 3 and 6). An alkylated cysteine preceded Pro 18, indicating the relative permissivity of the cyprose I for large groups at the S1 site. For Pro 18 and 47, residues at the S′2 site were, respectively, Gly and Pro. Cleavage at non-proline residues cannot be excluded but must be marginal because no corresponding peptides were detected.

Although there is no evidence to indicate that S91 in ECypP behaves like the nucleophile of serine proteases, we further introduced a histidine and an aspartic acid in ECypP-A91S to attempt to generate a catalytic triad-like machinery. ECypP-Q56S was not further investigated. A modelling study suggested F104 as the residue to be mutated into histidine because the imidazole group centre would be at 5.4 Å from the β-carbon of S91, as compared to 4.2 Å in a catalytic triad. ECyp-A91S-F104H was marginally more efficient than ECypP-A91S, with a 3.5-fold higher k_{cat} and a slight increase in the Michaelis constant ($K_m = 1.9$ mM).

Further modelling studies suggested that for the constraints of a catalytic triad to be approximately respected, an aspartic acid should preferably be introduced at position 106. EcypP-A91S-F104H-N106D was 20–23-fold more efficient than ECypP-A91S and ECypP-A91S-F104H, whereas the Michaelis constant remained similar to that of the double mutant. The k_{cat} of the triple mutant was nearly 100-fold higher than that of ECypP-A91S. In addition, its rate enhancement (k_{cat}/k_{uncat}) was about 10^9, a value comparable with those observed for a number of natural enzymes[14]. Furthermore, the *cis-trans* isomerase activity of the wild-type ECypP vanished upon introduction of the mutations A91S, F104H and N106D (data not shown), probably as a result of a lower hydro-

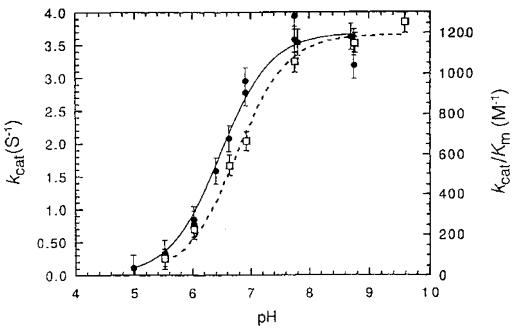

Figure 3 pH-rate profile of cyprose I. Hydrolysis of the model peptide fa-Ala-Pro was monitored spectrophotometrically in the presence of 1 and 100 nM enzyme, for determining, respectively, k_{cat} (●, solid line) and k_{cat}/K_m (□, dashed line). All measurements were performed in a mixed buffer consisting of 20 mM citrate phosphate borate at various pH levels. In this buffer, values for k_{cat} and k_{cat}/K_m measured at pH 8 were, respectively, $3.94 \pm 0.19\,s^{-1}$ and $1{,}192 \pm 59.3\,s^{-1}\,M^{-1}$, that is, 98.5% and 71.2% of those measured in the optimal buffer (Table 1). All values were corrected from the non-enzymatic hydrolysis which varied with pH. To calculate *p*K, both sets of data points were fitted to a single group titration model $y = y_{max}/(1 + 10^{pK-pH})$.

Table 1 Kinetic parameters for ECypP variants

	Efficiency k_{cat}/K_m ($s^{-1}M^{-1}$)	K_m ($\times 10^{-3}$ M)	k_{cat} (s^{-1})	Rate enhancement k_{cat}/k_{uncat}	Proficiency $(k_{cat}/K_m)/k_{uncat}$ (M)
WT	$<10^{-3}$	ND			
R48S	$<10^{-3}$	ND			
Q56S	$5.8 \pm 0.8 \times 10^{-3}$	ND			
A91S	73.1 ± 2.2	0.6 ± 0.15	0.044 ± 0.012	0.9×10^{7}	1.52×10^{10}
T93S	$<10^{-3}$	ND			
A91S-F104H	81.8 ± 3.3	1.9 ± 0.10	0.155 ± 0.015	3.23×10^{7}	1.70×10^{10}
A91S-F104H-N106D	1675 ± 12	2.4 ± 0.09	4.0 ± 0.2	8.33×10^{8}	0.35×10^{12}

First-order kinetics were determined spectrophotometrically for the single point variants and using both the spectrophotometric and the HPLC assays for the triple mutant in the best buffer system found (20 mM HEPES, pH 8.0). K_m and k_{cat} were deduced from the Wool-Augustinsson-Hofstee plot: v versus v/S (ref. 25).

phobicity in the enzyme active site[15]. Therefore, the three mutations sufficed to convert the peptidyl-prolyl isomerase ECypP into an efficient X-Pro peptidase. We called this new enzyme cyproase I.

We investigated the capacity of cyproase I to cleave the polypeptide chain of a snake curaremimetic toxin which contains 61 amino acids and four disulphide bonds, and includes five proline residues. The native toxin structure is resistant to proteolytic enzymes (such as cathepsins B and D[16]) and, as expected, cyproase I did not hydrolyse it. After reduction of the disulphide bonds and modification of the free cysteines, the toxin unfolds[17] and hence becomes cleavable by cyproase I. The peptides resulting from endoproteolysis were isolated by HPLC and characterized by Edman sequencing and electron spray mass spectrometry analysis (Fig. 2). Cleavages were observed before proline residues number 11, 18, 43 and 47. No cleavage between Pro-11 and Pro-12 was detected. Clearly, cyproase I not only cleaves the model fa-AP peptide but also displays an X-Pro-specific endoproteolytic activity. This enzyme may be of interest for future protein mapping.

How does this artificial proteolytic enzyme work? At present, we have no definite answer but a number of elements shed some light on this question. Thus, in the presence of 4-(2-aminoethyl)-benzenesulphonyl fluoride (AEBSF), cyproase I was completely inactivated within seconds (not shown), suggesting the involvement of a nucleophile in the catalytic mechanism. We suggest that S91 corresponds to this nucleophile residue, because introduction of the single mutation A91S was sufficient to generate an efficient proteolytic activity. Such a situation is not uncommon because some enzymes, including β-lactamases[18] and penicillin acylase[19], possess a nucleophilic serine in their active site despite having no catalytic triad. The residues that are responsible in ECypP-A91S for the nucleophilicity of S91 remain to be identified. What is perhaps more striking in our observation is that introduction of H104 and D106 further increased the efficiency of catalysis by a factor of 23. Although this value is substantially weaker than the corresponding effect observed in subtilisin[10], the data suggest a synergistic action between H104, D106 and S91. That a histidine residue participates directly in the catalytic mechanism of cyproase I is supported by the observation that a group titrates with a pK equal to 6.74 ± 0.16 and 6.74 ± 0.15, when measuring the k_{cat} and k_{cat}/K_m, respectively, versus pH (Fig. 3). Therefore the catalytic triad of cyproase I might share functional and structural similarities with conventional catalytic triads of serine proteases[7]. On the other hand, the examination of the structure of ECypP–peptide complex[2] suggested that the dyad H104–D106 might play the role of a general base, as in phospholipase A_2 (ref. 20). In this case, S91 would behave as an oxyanion hole motif.

There has been a constant demand for proteases with new specificity and protein engineering has been faced with this considerable challenge. Our results indicate that an alternative strategy based on modification of pre-existing enzymatic sites may lead to efficient and quite new activities. □

Method

The plasmid pJLEC-2B encoding *E. coli* periplasmic cyclophilin[21] was kindly provided by C. T. Walsh (Harvard Medical School, Boston). Site-directed mutagenesis was performed using Stratagene's QuickChange protocol. Cloning, sequencing and expression were made in the same plasmid construct and host strain (XL1-Blue, Stratagene). Protein production and purification of mutant proteins were achieved essentially as described[21], with minor modifications regarding chromatography supports. An additional gel filtration on Superdex 75 (Pharmacia Biotech) was added for mutants displaying peptidase activity.

The peptidase activity of mutants was first tested by a spectrophotometric assay derived from ref. 22. The furylacryloyl-alanylproline (fa-AP) substrate was synthesized from 3-(2-furyl)acryloyl-alanyl-*N*-hydroxysuccinimide ester and H-proline-2-chlorotrityl chloride resin (Bachem). A molar extinction coefficient of $13{,}400\,cm^{-1}M^{-1}$ at 300 nm was measured for fa-AP and its conversion was followed from the differential absorption spectra between fa-AP and fa-A at 324 nm ($\Delta\epsilon = -1{,}576\,cm^{-1}M^{-1}$). Mutant cyclophilin concentrations ranged from $50\,ng\,ml^{-1}$ to $5\,\mu g\,ml^{-1}$ in the assays whereas substrate concentrations were in the range 0–1 mM. Kinetic parameters were also determined from HPLC analysis of the reaction products on a μRPC-C2/C18 column (Pharmacia) at $0.3\,ml\,min^{-1}$, fa-Ala and fa-AP eluting, respectively, at 27.6 and 31.2% acetonitrile. Uncatalysed rate of fa-AP hydrolysis was determined by using HPLC to follow the evolution of the ratio of fa-AP/fa-A in a 20 mM fa-AP solution at 37 °C in 100 mM Tris-HCl buffer at pH 7.5 over a period of 45 days.

Toxin α from *Naja nigricollis* was reduced by 100 mM DTT, dialysed against 0.1 M acetic acid, and the eight cysteines were alkylated with 0.1 M *N*-ethylmaleimide in 50 mM Tris-Cl, pH 8.0. Hydrolysis was performed at 0.15 mM toxin in 20 mM HEPES, pH 7.0 in the presence of 0.11 μM cyproase I for 2 h at 37 °C. The products were lyophilized, resuspended in 0.1% TFA at $1\,mg\,ml^{-1}$ and characterized by HPLC (C18 Bondapak 3μ). Electron spray mass spectrometry analyses were performed at the mass spectrometry facility in DCC/SPEA, Saclay (H. Virelizier).

Received 4 June; accepted 13 October 1997.

1. Clubb, R. T., Ferguson, S. B., Walsh, C. T. & Wagner, G. Three-dimensional solution structure of *Escherichia coli* periplasmic cyclophilin. *Biochemistry* **33,** 2761–2772 (1994).
2. Konno, M., Ito, M., Hayano, T. & Takahashi, N. The substrate-binding site in *Escherichia coli* cyclophilin A preferably recognizes a *cis*-proline isomer or a highly distorted form of the *trans*-isomer. *J. Mol. Biol.* **256,** 897–908 (1996).
3. Zhao, Y. & Ke, H. Mechanistic implication of crystal structures of the cyclophilin-dipeptide complexes. *Biochemistry* **35,** 7362–7362 (1996).
4. Zhao, Y. & Ke, H. Crystal structure implies that cyclophilin predominantly catalyzes the *trans* to *cis* isomerization. *Biochemistry* **35,** 7356–7362 (1996).
5. Kirby, A. J. Enzyme mechanisms, models, and mimics. *Angew. Chem. Int. Ed. Engl.* **35,** 707–724 (1996).
6. Matthews, B. W., Craik, C. S. & Neurath, H. Can small cyclic peptides have the activity and specificity of proteolytic enzymes. *Proc. Natl Acad. Sci. USA* **91,** 4103–4105 (1994).
7. Fersht, A. *Enzyme Structure and Mechanism* (W. H. Freeman, New York, 1985).
8. Fischer, G., Wittmann-Liebold, B., Lang, K., Kiefhaber, T. & Schmid, F. X. Cyclophilin and peptidyl-prolyl *cis-trans* isomerase are probably identical proteins. *Nature* **337,** 476–478 (1989).
9. Galat, A. & Metcalfe, S. M. Peptidylproline *cis/trans* isomerases. *Prog. Biophys. Mol. Biol.* **63,** 69–119 (1995).
10. Carter, P. & Wells, J. A. Dissecting the catalytic triad of a serine protease. *Nature* **332,** 564–568 (1988).
11. Bode, W. & Huber, R. Natural protein proteinase inhibitors and their interaction with proteinase. *Eur. J. Biochem.* **204,** 433–451 (1992).
12. Gamble, T. R. *et al.* Crystal structure of human cyclophilin A bound to the amino-terminal domain of HIV-1 capsid. *Cell* **87,** 1285–1294 (1996).
13. Kahne, D. & Still, W. C. Hydrolysis of a peptide bond in neutral water. *J. Am. Chem. Soc.* **110,** 7529–7534 (1988).
14. Radzicka, A. & Wolfenden, R. A proficient enzyme. *Science* **267,** 90–93 (1995).
15. Stein, R. L. Mechanism of enzymatic and nonenzymatic prolyl cis-trans isomerization. *Adv. Prot. Chem.* **44,** 1–24 (1993).
16. Maillère, B. *et al.* Immunogenicity of a disulphide-containing neurotoxin: presentation to T-cells requires a reduction step. *Toxicon* **33,** 475–482 (1995).

17. Ménez, A., Montenay-Garestier, T., Fromageot, P. & Hélène, C. Conformation of two homologous neurotoxins. Fluorescence and circular dichroism studies. *Biochemistry* **19,** 5202–5208 (1980).
18. Strynadka, N. C. J. *et al*. Molecular structure of the acyl-enzyme intermediate in β-lactam hydrolysis at 1.7 Å resolution. *Nature* **359,** 700–705 (1992).
19. Duggleby, H. J. *et al*. Penicillin acylase has a single-amino-acid catalytic centre. *Nature* **373,** 264–268 (1995).
20. Scott, D. L. *et al*. Interfacial catalysis: the mechanism of phospholipase A2. *Nature* **250,** 1541–1546 (1990).
21. Liu, J. L. & Walsh, C. T. Peptidyl-prolyl *cis-trans* isomerase from *Escherichia coli*: A periplasmic homolog of cyclophilin that is not inhibited by cyclosporin A. *Proc. Natl Acad. Sci. USA* **87,** 4028–4032 (1990).
22. Plummer, T. H. Jr & Kimmel, M. T. An improved spectrophotometric assay for human carboxypeptidase N1. *Anal. Biochem.* **108,** 348–353 (1980).
23. Kraulis, P. Molscript: a program to produce both detailed and schematic plots of protein structures. *J. Appl. Crystallogr.* **24,** 946–950 (1991).
24. Merritt, E. A. & Murphy, M. Raster3D version 2.0—a program for photorealistic molecular graphics. *Acta Crystallogr. D* **50,** 869–873 (1994).
25. Segel, I. H. *Enzyme Kinetics: Behavior and Analysis of Rapid Equilibrium and Steady-state Enzyme Systems* (John Wiley, New York, 1993).

Acknowledgements. We thank J. Janin, F. Lederer and G. Robillard for useful and critical reading of the manuscript.

Correspondence and requests for materials should be addressed to E.Q. (e-mail: eric.quemeneur@cea.fr).

Visualizing DNA replication in a catalytically active *Bacillus* DNA polymerase crystal

James R. Kiefer*, Chen Mao*, Jeffrey C. Braman† & Lorena S. Beese*

** Department of Biochemistry, Box 3711, Duke University Medical Center, Durham, North Carolina 27710, USA*
† Stratagene, 11011 N. Torrey Pines Rd, La Jolla, California 92017, USA

DNA polymerases copy DNA templates with remarkably high fidelity, checking for correct base-pair formation both at nucleotide insertion and at subsequent DNA extension steps[1–3]. Despite extensive biochemical, genetic and structural studies[2,4], the mechanism by which nucleotides are correctly incorporated is not known. Here we present high-resolution crystal structures of a thermostable bacterial (*Bacillus stearothermophilus*) DNA polymerase I large fragment[5] with DNA primer templates bound productively at the polymerase active site. The active site retains catalytic activity, allowing direct observation of the products of several rounds of nucleotide incorporation. The polymerase also retains its ability to discriminate between correct and incorrectly paired nucleotides in the crystal. Comparison of the structures of successively translocated complexes allows the structural features for the sequence-independent molecular recognition of correctly formed base pairs to be deduced unambiguously. These include extensive interactions with the first four to five base pairs in the minor groove, location of the terminal base pair in a pocket of excellent steric complementarity favouring correct base-pair formation, and a conformational switch from B-form to underwound A-form DNA at the polymerase active site.

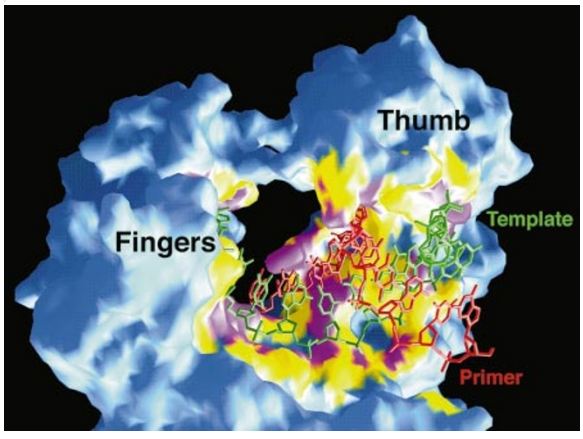

Figure 1 Structure of the *Bacillus* fragment with duplex DNA bound at the polymerase active site. The *Bacillus* fragment molecular surface is coloured according to its proximity to the DNA, with all points less than 3.5 Å coloured magenta, between 3.5 and 5.0 Å yellow, and greater than 5 Å blue. Bound water molecules were not included in this calculation.

We have determined at 1.8 Å resolution the co-crystal structures of the large (relative molecular mass (M_r) 67K) carboxy-terminal fragment[5] of the thermostable *Bacillus stearothermophilus* DNA polymerase I complexed with DNA primer templates bound at the polymerase active site. We believe that these structures provide the most detailed view of any polymerase DNA complexes yet determined (Fig. 1). The polymerase active-site region of the fragment shows extensive structural (0.65-Å root mean square deviation (r.m.s.d.) of Cα atoms) and sequence homology (49% identity) to the analogous Klenow fragment[6] from *Escherichia coli*, which has been the model system for determining polymerase structure and function for over a decade[2,4]. Furthermore, the DNA duplex binds to the polymerase domain through an extensive network of hydrogen bonds, ion pairs, and van der Waals contacts, involving more than 40 residues which are highly conserved in polymerases of the PolI family. In particular, the residues located in the DNA polymerase active site itself, and which have been shown to be important for catalysis in the Klenow fragment[7,8], are invariant in the *Bacillus* fragment as well as the other members of the PolI family[9]. Preliminary characterization of the *Bacillus* fragment[5] suggests that its enzymatic and biochemical activities are also similar to those of the Klenow fragment, although the *Bacillus* fragment is more processive, incorporating 112 nucleotides compared with 7.7 nucleotides for the Klenow fragment[7].

Bacillus-fragment co-crystals of a DNA duplex of nine base pairs (bp) with an AGAGA-5′ template overhang sequence were incubated with solutions containing the ddTTP nucleotide complementary to the first position in the overhang. The 1.9-Å resolution structure of the resulting complex clearly showed that the duplex DNA region increased from nine to ten base pairs (Fig. 2). At this resolution the DNA sequence could be read without ambiguity from the electron density, and revealed that a newly synthesized A:T (template:primer) base pair was bound at the active site in a position previously occupied by the G:C base pair of the initial substrate, indicating that the added nucleotide had been incorporated into the DNA. No density was apparent for the 3′-OH of the sugar at the new terminus, as expected because it had become a dideoxyribose. The ($F_o - F_c$) difference maps showed a pattern of peaks and holes around the DNA bases, indicating that the sequence had translocated by one base pair after incorporation. To investigate whether more than one catalytic turnover could occur in the crystal,

Table 1 Summary of DNA helical parameters

	Bacillus fragment 11-bp complex	B-DNA	A-DNA
Mean twist (°)	33	36	33
Mean rise (Å)	3.2	3.4	2.6
Roll (°)	3.5	0	6
Inclination (°)	1.8	–6	2.6
X-displacement (Å)	–1.4	0.2	–4.5
Sugar pucker	C2′/C3′-endo*	C2′-endo	C3′-endo
Minor-groove width/depth (Å)			
Mean	8.0/3.5	5.7/7.5†	11.0/2.8†
Distal end	7.0/4.3		
Active-site end	10.2/1.1		
Major-groove width/depth (Å)			
Mean	12.05/5.5	11.7/8.5†	2.7/13.5†
Distal end	9.6/5.8		
Active-site end	14.8/0.6		
Mean helical diameter (Å)	19.5	19	23

Bacillus fragment–DNA complex helical parameters were compiled using CURVES version 5.1 (ref. 28). Typical values for B-DNA and A-DNA are provided for comparison[29].
* Sugar pucker is C3′-endo for the first 4bp of DNA except the 3′-primer terminus. That residue and all others are C2′-endo.
† From ref. 30.